Hybrid compact–WENO finite difference scheme with radial basis function based shock detection method for hyperbolic conservation laws

Preprint · January 2018

DOI: 10.13140/RG.2.2.32422.83525

CITATIONS
0

READS
296

5 authors, including:

Wai Sun Don
Ocean University of China
89 PUBLICATIONS **3,373** CITATIONS
SEE PROFILE

Bao-Shan Wang
Ocean University of China
22 PUBLICATIONS **95** CITATIONS
SEE PROFILE

Zhen Gao
Ocean University of China
47 PUBLICATIONS **528** CITATIONS
SEE PROFILE

Xiao Wen
Ocean University of China
9 PUBLICATIONS **66** CITATIONS
SEE PROFILE

Hybrid compact-WENO finite difference scheme with radial basis function based shock detection method for hyperbolic conservation laws

B.S. Wang *Z. Gao †Y.H. Wang ‡X. Wen §W.S. Don ¶

Abstract

Hybrid scheme, based on the high order nonlinear characteristic-wise weighted essentially non-oscillatory (WENO) conservative finite difference scheme and the spectral-like linear compact finite difference scheme, has been developed for capturing shocks and strong gradients accurately and resolving fine scale structures efficiently for hyperbolic conservation laws. The key issue in any hybrid scheme is the design of an accurate, robust, and efficient high order shock detection algorithm which is capable of determining the smoothness of the solution at any given grid point and time. An improved iterative adaptive multi-quadric radial basis function (IAMQ-RBF-Fast) method [Don et al. doi.org/10.1007/s10915-017-0572-y (2017)] has been successfully developed as an edges detector of the piecewise smooth functions. In this study, we address and resolve several technical challenges with state-of-arts numerical techniques, such as reducing the ill-condition of the large Toeplitz matrix system via domain rescaling, improving the efficiency of finding the inverse of Toeplitz matrix via the recursive Levinson-Durbin method and domain decomposition, increasing the robustness of the shock detection algorithm by employing the Tukey's boxplot method, yielding an accurate, robust and efficient RBF shock detection method. The applicability and performance of the RBF edge detection method as the shock detector in the hybrid scheme in terms of accuracy, robustness, efficiency, resolution and other implementation issues is studied in detail. Several one- and two-dimensional benchmark problems in shocked flow demonstrate that the proposed hybrid scheme can reach a speedup of the CPU times by a factor up to 2-3 compared with the pure fifth order WENO-Z scheme.

Keywords

*School of Mathematical Sciences, Ocean University of China, Qingdao, China. E-Mail: wbs@stu.ouc.edu.cn

†School of Mathematical Sciences, Ocean University of China, Qingdao, China. E-Mail: zhengao@ouc.edu.cn

‡College of Oceanic and Atmospheric Sciences, Ocean University of China, Qingdao, China. E-Mail: wangyinghua@stu.ouc.edu.cn

§College of Oceanic and Atmospheric Sciences, Ocean University of China, Qingdao, China. E-Mail: wenxiao@stu.ouc.edu.cn

¶Correspondence author: School of Mathematical Sciences, Ocean University of China, Qingdao, China. E-Mail: donwaisun@outlook.com

WENO-Z; Compact; Hybrid; Radial basis function; Outliers-detection; Tukey's boxplot; Hyperbolic

1 Introduction

Characteristic-wise weighted essentially non-oscillatory (WENO) conservative finite difference schemes on a uniformly spaced grid, as a class of high order/resolution nonlinear scheme for solutions of hyperbolic conservation laws in a Cartesian domain, namely, in the form of

$$\frac{\partial \mathbf{Q}}{\partial t} + \mathbf{F}(\mathbf{Q})_x + \mathbf{G}(\mathbf{Q})_y = 0, \quad x, y \in \mathbf{\Omega}, \tag{1}$$

in the presence of shocks and small scale structures, was initially developed by [16] (for details and history of the WENO scheme, see [1, 3, 24] and references therein). However, the WENO scheme is fairly complex to implement, computationally expensive and too dissipative for certain classes of problems. A natural way to alleviate some of these difficulties is to construct a hybrid scheme conjugating a nonlinear WENO scheme in the non-smooth stencils with a linear method in the smooth stencils [5, 10, 21, 22, 34]. The key issue in any hybrid scheme is the design of an *accurate*, *robust*, and *efficient high order* shock detection method that is capable of determining the smoothness of the solution at any given grid point and at any given time. Therefore, many shock detection methods have been developed, such as the low order shock detection methods, the TVB algorithm [4], the KXRCF [20], and the high order polynomial based multi-resolution analysis (MR) [5, 6, 10, 12], trigonometric based conjugate Fourier analysis [7], and the radial basis function based edge detection algorithm, which is the subject of this research.

Radial basis function (RBF) methods have been widely used in various important application areas, such as machine learning and neural networks [31], image processing, edge detection and piecewise smooth function reconstruction [17, 18], and numerical approximations of partial differential equations (PDEs) [2, 19]. A fast rate of convergence can be obtained in the RBF approximation if the given function is sufficiently smooth [32]. Otherwise, its rate of convergence deteriorates rapidly unless the centers or the shape parameters of the RBF are adapted accordingly.

In [17, 18], an iterative adaptive multi-quadric RBF (IAMQ-RBF) method has been designed for the one- and two-dimensional edges detection of a piecewise analytical function, which performs very well in detecting multiple local jump discontinuities on uniformly spaced centers. However, this results in an intensive CPU consuming computation of solving a perturbed Toeplitz matrix system at each iteration, which is in particularly inefficient for a large number of uniformly spaced centers. Therefore, we have proposed a fast direct solver, IAMQ-RBF-Fast method [8], that solves the perturbed Toeplitz matrix system by first decomposing the system via the Sherman-Morrison-Woodbury method and then solving the resulting two Toeplitz matrix systems via the $O(N^2)$ Levinson-Durbin recursive algorithm which utilizes the Yule-Walker algorithm [13]. However, it is still too expensive to be used as a shock detector in the hybrid scheme for solving the hyperbolic conservation laws [8].

In this followup work, we investigate the applicability of the RBF approximation as the shock de-

tector in the high order hybrid Compact-WENO scheme for solving hyperbolic PDEs and discuss its accuracy, robustness, efficiency, and other implementation issues in detail. Developing an efficient RBF shock detection method is not a trivial task, especially for high order methods. One key difficulty encountered in the RBF approximation is that the Toeplitz matrix is ill-conditioning for large number of grid points N and computing its inverse takes up much CPU time. To mitigate this issue, the domain decomposition technique [33] is employed to uniformly subdivide the whole computational domain into N_S subdomains containing N_k elements each, and then the RBF approximation is used in each subdomain. The subdomain partition reduces the ill-conditioning while increases the overall computational efficiently in solving a much smaller matrix system. The dominant and large RBF approximation error at the subdomain boundaries can be mitigated by three points overlapping with its neighboring subdomains. Another important complication in developing an efficient RBF shock detection method comes from the fact that the most time consuming part in the IAMQ-RBF-Fast method [8] is solving the Toeplitz matrix system at each iterative step. To further increase the efficiency of the RBF-based shock detection algorithm, as an alternative to the iterative process of IAMQ-RBF-Fast algorithm, it is sufficient to perform the iteration once (twice if necessary) and then employ the outliers detection algorithm [11, 29] to accurately identify the locations of shocks and high gradients for most of the problems tested. Several classical one- and two-dimensional benchmark problems of shocked flows verify the performance (in terms of accuracy, resolution, rebustness, and efficiency) of the hybrid Compact-WENO scheme with the RBF shock detection method when compared with the pure WENO-Z scheme and the hybrid scheme with the multi-resolution analysis based shock detection method.

This paper is organized as follows. We begin in Section 2 with a brief introduction to the algorithm of hybrid Compact-WENO finite difference scheme and continue in Section 3 with the multi-quadric RBF approximation and the fast method for computing the inverse of the Toeplitz matrix. In Section 4, the Tukey's boxplot method and improved outliers detection algorithm are briefly reviewed. The RBF shock detection method for the hybrid Compact-WENO finite difference scheme for hyperbolic conservation laws, on the basis of the segmented RBF approximation and outliers detection algorithm is described in Section 5. In Section 6, several classical one- and two-dimensional shocked problems are simulated and their results are discussed. Concluding remarks are given in Section 7.

2 The hybrid Compact-WENO Finite Difference Scheme

In this section, we outline the temporal-spatial adaptive algorithm of the higher order hybrid Compact-WENO finite difference scheme that is used for solving the Euler equations [7]. The implementation of the numerical schemes (the sixth order central compact finite difference scheme, the fifth order ($2r-1=5$) characteristic-wise WENO-Z finite difference scheme with the global[1] Lax-Fredrichs flux splitting via the Roe averaged eigensystem, the sixth order finite difference fil-

[1]The maximum is taken over all the absolute value of the eigenvalues of the system and over the local WENO non-smooth region $\mathbf{\Omega}_{\text{WENO}}$ where the grid point is belonged to (see below), instead of over the whole global physical domain $\mathbf{\Omega}$.

tering and the third order Runge-Kutta TVD scheme) used in this study are well described in great details in [7] and will be omitted in this paper. Other temporal-spatial adaptive hybrid algorithms using different shock-detection algorithms/trouble cell indicators, for example [5, 10] can also be used.

The hybrid algorithm consists of four main steps that, 1) at a beginning of a Runge-Kutta time step, determine the smoothness of solution at a given grid point by a shock detection algorithm, 2) markup the non-smooth grid points with a Flag, 3) setup a buffer zone around the non-smooth grid point, 4) determine the derivative of the flux with the WENO scheme at the non-smooth stencils and with the compact scheme otherwise, and, 5) at the end of the Runge-Kutta time step, stabilize the solution by a finite difference filtering in the smooth stencils if needed.

Algorithm: (Hybrid Compact-WENO finite difference scheme)

1. Perform the smoothness analysis of the solution (typically, density ρ) via a shock-detection algorithm (for example, multi-resolution analysis) once at the beginning of the Runge-Kutta scheme.

2. Set a flag at a grid point x_i as

$$\text{Flag} = \begin{cases} 1, & (\text{ Non-smooth stencil}), \\ 0, & (\text{ Smooth stencil}), \end{cases}$$

   as determined by RBF shock detection method (see Section 5).

3. Create a buffer zone around each non-smooth grid point x_i such that all the grid points inside the buffer zone are flagged as the non-smooth stencils $\mathbf{\Omega}_{\text{WENO}}$, else the smooth stencils $\mathbf{\Omega}_{\text{compact}}$.

   If, for example, a grid point x_i is flagged as a non-smooth stencil, then its neighboring grid points $\{x_{i-m}, \ldots, x_i, \ldots, x_{i+m}\}$ will also be designated as the non-smooth stencils. (Typically, $m = r$).

4. Compute the derivative of the fluxes at each cell center by

   - (Non-smooth WENO stencils $\mathbf{\Omega}_{\text{WENO}}$): the WENO-Z scheme.
   - (Smooth compact stencils $\mathbf{\Omega}_{\text{compact}}$): the compact scheme.

   The numerical fluxes on the non-smooth stencils obtained by the WENO-Z scheme are saved and automatically used as the internal boundary fluxes needed by the compact scheme. The numerical fluxes near the domain boundary are also computed by the WENO-Z scheme.

5. Stabilize the Hybrid scheme.

   An sixth order finite difference filtering [27] is applied in the smooth stencils to stabilize the hybrid Compact-WENO scheme.

Remark 1 *This step can be skipped if the upwind Compact finite difference scheme [21] is used instead of the central one.*

Remark 2 *Before creating a buffer zone, if a smooth stencil sandwiched between two non-smooth stencils has less than* $(2m + r)$ *grid points, the smooth stencil is merged together with its two neighboring non-smooth stencils to form a single contiguous non-smooth stencil. The reasons are 1) a* $2m\_th$ *order compact scheme would need at least* $(2m - 1)$ *grid points to obtain its optimal order, and 2), simultaneously, this extra step reduces the fragmentation of the WENO non-smooth regions, which in turn reduces the cache miss and improves the vectorization of the compiled program, thus increases the overall efficiency of the hybrid scheme. This is where this version of hybrid scheme departs from our previous version [7].*

3 Multi-Quadric Radial Basis Function (MQ-RBF)

A radial basis function (RBF) is defined on a set of centers $\mathbf{X} = \{x_i \mid x_i \in \mathbf{\Omega},\ i = 1, \cdots, N\}$ and a set of corresponding shape parameters $\epsilon_i,\ i = 1, \cdots, N$. In the given domain, a set of function values $\vec{f} = (f_1, \cdots, f_N)^T$, where $f_i = f(x_i)$, is also given.

In this study, we consider the multi-quadric radial basis function (MQ-RBF)

$$\phi_i(x) = \sqrt{(x - x_i)^2 + \epsilon_i^2},\ x_i \in \mathbf{X},\ x \in \mathbf{\Omega},\ i = 1, \cdots, N,$$

where the shape parameter $\epsilon_i \geq 0$ is a real (or complex) number that may be a constant for all centers x_i, determined by the priori approximation or adaptively determined according to the characteristics of the given function at each center x_i. As shown later, the shape parameter ϵ_i plays a critical role in the development of the shock detection algorithm when its value is changed adaptively according to the local smoothness of the function.

The MQ-RBF approximation $g(x)$ and its derivative $g'(x)$ for a real-valued function $f(x)$ are given by

$$g(x) = \sum_{i=1}^{N} \lambda_i \phi_i(x), \quad g'(x) = \sum_{i=1}^{N} \lambda_i \frac{x - x_i}{\phi_i(x)}, \tag{2}$$

where λ_i are the RBF coefficients. The RBF coefficients $\vec{\lambda} = (\lambda_1, \cdots, \lambda_N)^T$ are obtained by enforcing the interpolation conditions $g(x_i) = f(x_i), \forall x_i \in \mathbf{X}$, that is,

$$\vec{\lambda} = \mathbf{M}^{-1} \vec{f}, \tag{3}$$

where the interpolation matrix $\mathbf{M}$ has the elements $M_{ij} = \sqrt{(x_i - x_j)^2 + \epsilon_j^2}$.

The derivative, when evaluated at the center x_i, the vector $\vec{g'} = (g'(x_1), \cdots, g'(x_N))^T$, becomes

$$\vec{g'} = \mathbf{D}\vec{\lambda} = \mathbf{D}\mathbf{M}^{-1} \vec{f}, \tag{4}$$

where the differentiation matrix $\mathbf{D}$ has the elements $D_{ij} = (x_i - x_j)/M_{ij}$ if $\epsilon_j \neq 0$ and $D_{ii} = 0$ if $\epsilon_i = 0$.

Remark 3 *We rewrite the function $f(x) = \hat{f}(x) + mean(f(x))$, and then approximate the function $\hat{f}(x)$ and its derivative, which is equal to the derivative of $f(x)$, by the RBF.*

We will now give the definitions of the normalized concentration map and edges set which are used in the edges detections [8, 17].

Definition 4 *The normalized concentration map $\mathbf{C} = \{C_i,\ i = 1, \cdots, N\}$ is defined by*

$$C_i = \frac{\hat{C}_i}{\max\{\hat{C}_i\}}\ , \textit{where}\ \hat{C}_i = \left|\lambda_i \sum_{j=1}^{n} D_{ij}\lambda_j\right|,\ \ i = 1, \cdots, N. \tag{5}$$

The normalized concentration map $\mathbf{C}$ measures the smoothness of the solution. A simple way to identify the location of a discontinuity at x_i is where the C_i is larger than a user defined parameter η and $g_i' \neq 0$. This leads us to the definition of the non-smooth centers.

Definition 5 *The edges set $\mathbf{S}_{RBF}$ is defined as*

$$\mathbf{S}_{RBF} = \{x_i \mid C_i \geq \eta,\ g_i' \neq 0,\ x_i \in \mathbf{X},\ i = 1, \cdots, N\}, \tag{6}$$

where $\eta \in (0, 1)$ is the given tolerance parameter.

The edge set $\mathbf{S}_{RBF}$ contains all the centers which are identified as edges/boundaries/sharp gradients. A typical robust $\eta = 0.5$ is used in [17].

Alternatively, the scales $d_i = |g_i|^2$ can also be used to measure the smoothness of a function.

Definition 6 *The edges set $\mathbf{S}_{RT}$ is defined as*

$$\mathbf{S}_{RT} = \{x_i \mid d_i \geq \zeta,\ d_i = |g_i|^2,\ x_i \in \mathbf{X},\ i = 1, \cdots, N\}, \tag{7}$$

where d_i is referred as the RBF scales and $\zeta > 0$ is the given tolerance parameter.

However, its performance in detecting discontinuities is sensitive to the choice of ζ, which is usually a problem dependent parameter. In this study, the outliers detection algorithm based on the Tukey's boxplot method (see Section 4 below) is used to remove the need of specifying the parameter ζ.

3.1 Inverse of the Toeplitz Matrix via the $O(N^2)$ Recursive Levinson-Durbin Algorithm

For simplicity, we denote the RBF interpolation matrix $\mathbf{M}$ in Eqs. (3) and (4) as $\mathbf{T}_N$ which is a symmetric Toeplitz matrix provided $\epsilon_i = \epsilon > 0$ with N rows and columns. The Toeplitz matrix system can be written generically as

$$\mathbf{T}_N \vec{x} = \begin{pmatrix} 1 & \gamma_1 & \cdots & \gamma_{N-1} \\ \gamma_1 & 1 & \ddots & \vdots \\ \vdots & \ddots & \ddots & \gamma_1 \\ \gamma_{N-1} & \cdots & \gamma_1 & 1 \end{pmatrix} \begin{pmatrix} x_1 \\ x_2 \\ \vdots \\ x_N \end{pmatrix} = \vec{b}, \tag{8}$$

which can be solved directly by the $O(N^3)$ Gaussian elimination algorithm. However, it can become computationally expensive for large N. Instead, the $O(N^2)$ recursive Levinson-Durbin algorithm which utilized the recursive Yule-Walker algorithm can be employed to greatly improve the efficiency in finding the inverse of the Toeplitz matrix T_N^{-1}. In the following discussion, $\mathbf{I}_k \in \mathbb{R}^{k\times k}$ and $\mathbf{J}_k \in \mathbb{R}^{k\times k}$ are the identity and backward identity (exchange) matrices, respectively.

- First, the recursive Yule-Walker algorithm [13] is employed to solve the modified Toeplitz system in the form of

$$\mathbf{T}_k \vec{x} = -\vec{r}_k = -(\gamma_1, \cdots, \gamma_{k-1}, \gamma_k)^T, \tag{9}$$

  where $\gamma_i \in \mathbb{R}$ is the value of i-th off-diagonal of $\mathbf{T}_k$ $(1 \le i \le k-1)$, and $\gamma_k \in \mathbb{R}$ is any given real number.

  If $\vec{y}_k$ is the solution of Eq. (9), the $O(N^2)$ recursive Yule-Walker algorithm finds the solution $\vec{y}_{k+1}$ of the modified Toeplitz system

$$\mathbf{T}_{k+1}\vec{y}_{k+1} = -\vec{r}_{k+1} = (\gamma_1, \cdots, \gamma_k, \gamma_{k+1})^T. \tag{10}$$

  By rewriting $\vec{y}_{k+1} = (\vec{z}_k^T, a_k)^T$, Eq. (10) can be reformulated as

$$\begin{pmatrix} \mathbf{T}_k & \mathbf{J}_k\vec{r}_k \\ \vec{r}_k^T\mathbf{J}_k & 1 \end{pmatrix} \begin{pmatrix} \vec{z}_k \\ a_k \end{pmatrix} = -\begin{pmatrix} \vec{r}_k \\ \gamma_{k+1} \end{pmatrix}.$$

  Since $\mathbf{T}_k^{-1}\mathbf{J}_k = \mathbf{J}_k\mathbf{T}_k^{-1}$, one has the solution $\vec{y}_{k+1} = (\vec{z}_k^T, a_k)^T$ with

$$a_k = -(\gamma_{k+1} + \vec{r}_k^T\mathbf{J}_k\vec{y}_k)/\delta_k, \quad \vec{z}_k = (\mathbf{I}_k + a_k\mathbf{J}_k)\vec{y}_k, \tag{11}$$

  where $\delta_k = 1 + \vec{r}_k^T\vec{y}_k$, which satisfies the recursion relationship $\delta_{k+1} = (1 - a_k^2)\delta_k$.

  In summary, given the initial solution $(k = 1, \vec{y}_1 = a_1 = -\gamma_1, \delta_1 = 1)$, the solution $\vec{y}_{k+1} = (\vec{z}_k^T, a_k)^T$ can be obtained via Eqs. (11) by recursion with $O(N^2)$ floating point operations.

- Next, a recursive Levinson-Durbin algorithm is employed to find the inverse of $\mathbf{T}_{k+1}$,

$$\mathbf{T}_{k+1}^{-1} = \begin{pmatrix} \mathbf{T}_k & \mathbf{J}_k\vec{r}_k \\ \vec{r}_k^T\mathbf{J}_k & 1 \end{pmatrix}^{-1} = \begin{pmatrix} \mathbf{H}_k & \vec{\nu} \\ \vec{\nu}^T & \sigma \end{pmatrix}.$$

From $\mathbf{T}_k\vec{\nu} + \sigma\mathbf{J}_k\vec{r}_k = \vec{0}$ and $\vec{r}_k^T\mathbf{T}_k\vec{\nu} + \sigma = 1$, one obtains

$$\sigma = 1/\delta_k, \quad \vec{\nu} = \sigma\mathbf{J}_k\vec{y}_k, \tag{12}$$

where $\vec{y}_k$ is the solution of modified Toeplitz system via the Yule-Walker algorithm.

From $\mathbf{T}_k\mathbf{H}_k + \mathbf{J}_k\vec{r}_k\vec{\nu}^T = \mathbf{I}_k$, one has

$$\mathbf{H}_k = \mathbf{T}_k^{-1} - \mathbf{T}_k^{-1}\mathbf{J}_k\vec{r}_k\vec{\nu}^T = \mathbf{T}_k^{-1} + \vec{\nu}\vec{\nu}^T/\sigma, \tag{13}$$

where the last term is derived from $\mathbf{T}_k^{-1}\mathbf{J}_k\vec{r}_k = -\mathbf{J}_k\vec{y}_k$ and Eq. (12).

Since $\mathbf{T}_k^{-1} = [t_{ij}]$ is a persymmetric matrix, that is, $t_{ij} = t_{k+1-j,k+1-i}$, the element of $\mathbf{H}_k$ is

$$h_{ij} = t_{ij} + \nu_i\nu_j/\sigma = h_{k+1-j,k+1-i} + (\nu_i\nu_j - \nu_{k+1-i}\nu_{k+1-j})/\sigma, \quad i,j = 1,\cdots,k. \tag{14}$$

Using the persymmetric property of $\mathbf{T}_{k+1}^{-1}$, and Eq. (14), all the elements of $\mathbf{T}_{k+1}^{-1}$ can be successively found by recursion.

3.2 Fast Iterative Adaptive MQ-RBF Method

To detect all the possible edges of a piecewise smooth function, the *iterative adaptive* MQ-RBF (IAMQ-RBF) method first detects the edge set $\mathbf{S}_{RBF}$ with a constant shape parameter ($\epsilon_i = \epsilon$) and then reset all the corresponding shape parameter $\epsilon_i = 0$. The RBF coefficient λ_i where $x_i \in \mathbf{S}_{RBF}$ becomes algebraically small, thus the new large λ_i in the next iteration will form a new edge set. This iterative process repeats itself and terminates if the number of iteration k is greater than n, or the residual norm of the RBF coefficients of the successive iterations is smaller than a given tolerance δ, that is, $||\vec{\lambda}^{k+1} - \vec{\lambda}^k||_2 \le \delta$, where $\vec{\lambda}^{k+1}$ and $\vec{\lambda}^k$ are the coefficient vectors at the $(k+1)$ and k iterative steps. Here the residual norm tolerance is $\delta = 10^{-8}$.

In an iteration step $k > 1$ of the IAMQ-RBF method, $\mathbf{M}_k$ is obtained by updating some shape parameter ϵ_i, says $\epsilon_{N_j} = 0$ and $\mathbf{M}_k$ is no longer a symmetric Toeplitz matrix but a perturbed Toeplitz (Toeplitz-ϵ) matrix. In this case, the fast direct solver described above cannot be applied directly. For example, $\mathbf{M}_1$ is no longer a symmetric Toeplitz matrix but a Toeplitz-ϵ matrix,

$$\mathbf{M}_1 = \mathbf{T} + \mathbf{E}, \tag{15}$$

where

$$\mathbf{T} = \begin{pmatrix} r_0 & r_1 & \cdots & r_{N-1} \\ r_1 & r_0 & \ddots & \vdots \\ \vdots & \ddots & \ddots & r_1 \\ r_{N-1} & \cdots & r_1 & r_0 \end{pmatrix}, \ \mathbf{E} = \begin{pmatrix} 0 & \cdots & 0 & s_{1,N_j} & 0 & \cdots & 0 \\ 0 & \cdots & 0 & s_{2,N_j} & 0 & \cdots & 0 \\ \vdots & & \vdots & \vdots & \vdots & & \vdots \\ 0 & \cdots & 0 & s_{N,N_j} & 0 & \cdots & 0 \end{pmatrix}, \tag{16}$$

where $r_i = \sqrt{(i\Delta x)^2 + \epsilon^2}$ and $s_{ij} = |x_i - x_j| - \mathbf{T}_{ij}$. Hence, at each iteration step of the IAMQ-RBF method, one needs to solve a new Toeplitz-ϵ matrix system with a known right hand side $\vec{b}$,

$$(\mathbf{T} + \mathbf{E})\vec{x} = \vec{b}, \tag{17}$$

where $\mathbf{T} \in \mathbb{R}^{N\times N}$, and $\mathbf{E} \in \mathbb{R}^{N\times N}$ is a zero matrix except its columns $N_1, N_2, \cdots, N_m$ and $m \ll N$. The key observation here is that the matrix $\mathbf{E}$ can be expressed as a product of two rank-m matrices $\mathbf{G}$ and $\mathbf{P}$ as

$$\mathbf{E} = \mathbf{G}\mathbf{P}^T, \tag{18}$$

where $\mathbf{G} \in \mathbb{R}^{N\times m}$ with the columns being the non-zero columns of $\mathbf{E}$, and $\mathbf{P} = (\vec{e}_{N_1}, \cdots, \vec{e}_{N_m}), \in \mathbb{R}^{N\times m}$ being a permutation matrix with $\vec{e}_j \in \mathbb{R}^{N\times 1}$ being the j-th unit column vector.

- By applying the Sherman-Morrison-Woodbury formula, one has

$$(\mathbf{T} + \mathbf{G}\mathbf{P}^T)^{-1} = \mathbf{T}^{-1} - \mathbf{T}^{-1}\mathbf{G}(\mathbf{I}_m + \mathbf{P}^T\mathbf{T}^{-1}\mathbf{G})^{-1}\mathbf{P}^T\mathbf{T}^{-1}, \tag{19}$$

  where $\mathbf{I}_m \in \mathbb{R}^{m\times m}$ is the identity matrix.

  Thus, one only needs to solve two Toeplitz matrix systems

$$\mathbf{T}\mathbf{U} = \mathbf{G}, \quad \mathbf{T}\vec{v} = \vec{b}, \tag{20}$$

  and a small $(m \times m)$ linear system

$$\mathbf{B}\vec{w} = \mathbf{P}^T\vec{v}, \tag{21}$$

  where $\mathbf{B} = \mathbf{I}_m + \mathbf{P}^T\mathbf{U} \in \mathbb{R}^{m\times m}$, to obtain the solution of Eq. (17) as

$$\vec{x} = \vec{v} - \mathbf{U}\vec{w}. \tag{22}$$

Remark 7

1. *The $O(m^3)$ Gaussian elimination method is used for solving the small linear system Eq. (21). Since $m \ll N$, it incurs only a small increase in the computational cost in solving Eq. (17).*

2. *Since the Toeplitz matrix $\mathbf{T}$ and $\vec{b}$ in Eq. (20) do not change in each iteration, the solution $\vec{v}$ can be first computed once and stored for a later use to save additional computational cost.*

Hence, the Toeplitz-ϵ matrix system is reduced to finding a fast direct solver for finding the inverse of the Toeplitz matrix $\mathbf{T}$, $\mathbf{T}^{-1}$. Therefore, instead of the $O(N^3)$ Gaussian elimination method, $\mathbf{T}^{-1}$ can be computed by the $O(N^2)$ recursive Levinson-Durbin algorithm as described in section 3.1. We refer to the IAMQ-RBF method with the $O(N^2)$ fast direct solver as the IAMQ-RBF-Fast method [8].

To illustrate the performance of the IAMQ-RBF-Fast method [8], we consider the two-dimensional Shepp-Logan phantom image and the edges detected by the IAMQ-RBF-Fast method as shown in

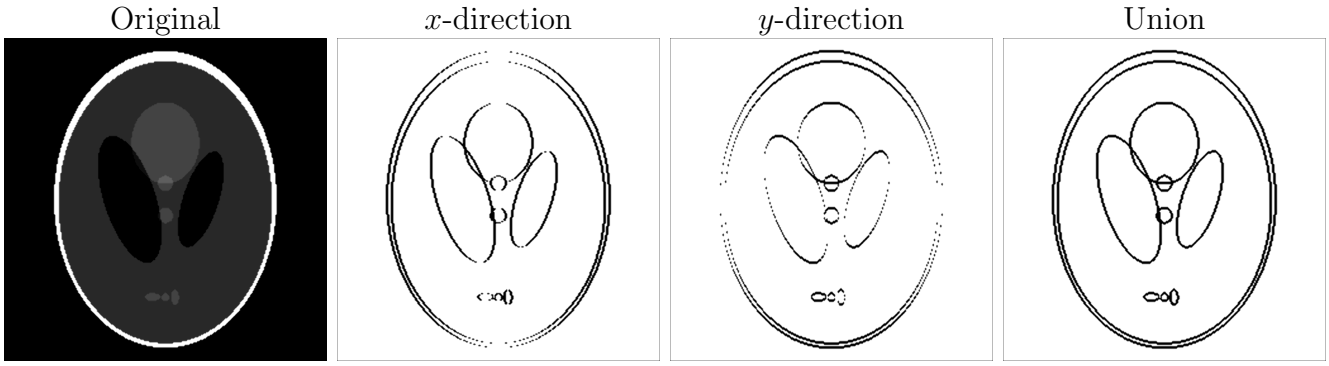

Figure 1: Final edges of the Shepp-Logan image with the size of 256×256. Left: The original image. Right: The edges detected by the IAMQ-RBF-Fast method with $\epsilon = 0.1, \eta = 0.01$.

Fig. 1. One can easily see that the IAMQ-RBF-Fast method works very well and efficiently in detecting edges with both large and small jumps.

With additional improvements and modifications as discussed below, the RBF edge detection method has an excellent potential to be a tool for identifying sharp gradients and shocks in a hybrid scheme.

3.3 Reducing Ill-conditioning via Domain Decomposition

It is well-known that the interpolation matrix $\mathbf{M}$ is ill-conditioning for large N. There are two remedies for mitigating the exponential growth of the condition number $\kappa(\mathbf{M})$ with large N. One approach is re-scaling the domain interval [18]. Another approach is the domain decomposition technique [33] in which the whole domain $\mathbf{\Omega}$, discretized with N uniformly spaced grid points, is uniformly divided into N_S sub-domains $\mathbf{\Omega}_k,\ k = 1, \cdots, N_S$, each containing N_k elements, and then the RBF approximation is used in $\mathbf{\Omega}_k$. As an added bonus, the domain decomposition technique also results in reducing CPU timings. For example, consider a constant function $f(x) = 1$, the CPU times with different N_k by repeating the approximation 1000 times are shown in the left figure of Fig. 2. It is clearly observed that smaller size matrices need less CPU time. The L^∞ errors between the exact and numerical solutions are plotted in the right figure of Fig. 2. Here, three overlapping points between two subdomains are also used to reduce the L^∞ errors around the interfaces. The result shows that the L^∞ errors are about ten times less than those without overlapping points. By considering the balance between accuracy and CPU time, we choose $N_k = 100$ in this work.

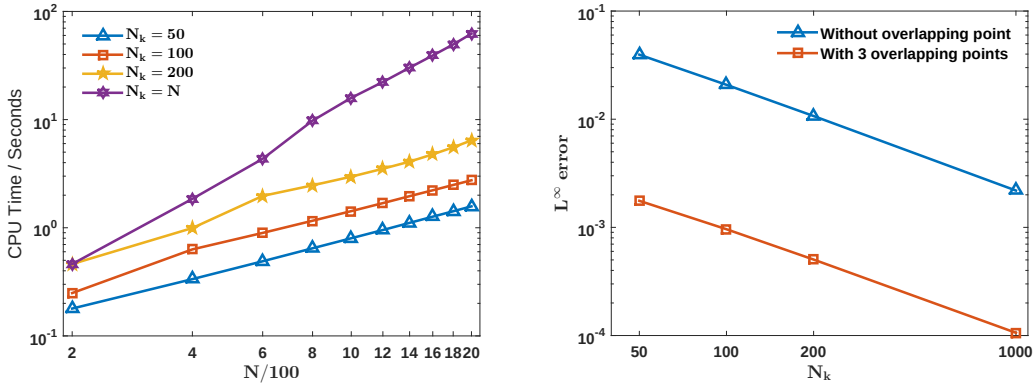

Figure 2: (Left) The total CPU timings, and (Right) mean of L^∞ errors with different number of elements N_k in a subdomain.

4 The Outliers Detection Algorithm with the Tukey's boxplot method

The user tunable parameter ζ in Definition 6 plays an important role in the performance of the RBF shock detection method. Clearly, ζ should be a problem dependent parameter and its optimal choice requires some subjective tuning. In order to increase the robustness of the shock detection method, the troubled-cell indicator proposed by [29] that uses the statistical approach in data analysis, or more specifically, the Tukey's boxplot method, seems very promising. A Tukey's boxplot method is often used to detect *outliers* of data in statistics [9, 26, 28]. The outliers are those data that fall far away from the median of the data set. We hypothesize here that discontinuities or shocks are singular and rare energetic finite events in the solution of hyperbolic conservation laws and behave like the outliers. One key property of this method is that most if not all 'false positives', if any, can be eliminated if the distribution of data is well behaved (i.e., Gaussian [14]). Another important property is that it is not necessary to specify the number of possible outliers in advance.

Here, we will briefly review an outliers detection (OD) algorithm as proposed in [29], which was used as the troubled-cell indicator for finding troubled cells in the discontinuous Galerkin (DG) method (see [11] for the detailed descriptions of the improved outliers detection algorithm.)

We begin by introducing the definitions of quartiles in statistics. Given a data set $\mathbf{d} = (d_0, d_1, \ldots, d_N)$, it is first sorted in an ascending order to form a new data set $\mathbf{d}^s = (d_0^s, d_1^s, \ldots, d_N^s)$, where $d_0^s \le d_1^s \le \ldots \le d_N^s$. The first quartile $Q_1 = (1-g)d_{j-1}^s + gd_j^s$, with $g = j - 1 - \lfloor N/2 \rfloor$, is the middle between the smallest value and the median of $\mathbf{d}^s$. The third quartile Q_3 is defined correspondingly as the middle between the largest value and the median of $\mathbf{d}^s$.

To identify the potential outlier(s) in the data set $\mathbf{d}^s$, fences $F_1 = \min\{-Q_{\text{mean}}, Q_1 - 3\Delta Q\}$ and $F_3 = \max\{Q_{\text{mean}}, Q_3 + 3\Delta Q\}$, where $Q_{\text{mean}} = (\sum_{i=0}^{N} |d_i|)/(N+1)$ measures the global mean

energy of the data and $\Delta Q = Q_3 - Q_1$ as proposed by Tukey [26], are defined. When the solution is relatively smooth, d_i is relatively small, which in turn implies that Q_{mean} is also substantially small. The appearance of shock will increase the d_i to a large value and Q_{mean} will correspondingly increase substantially (see [7, 11] for details and examples). Using the fences, one defines the domain $\Omega_f = [F_1, F_3]$. With these definitions, any data d_k^s that lies outside Ω_f ($d_k^s \notin \Omega_f$) is considered to be an outlier and we set the WENO flag at its corresponding grid point $\text{Flag}_{i(k)} = 1$, where $i(k)$ is the grid index corresponding to the original data set $\mathbf{d}$ before sorting. Otherwise, we set $\text{Flag}_{i(k)} = 0$.

The outliers detection algorithm can be applied to the RBF scales $\mathbf{d} = |\vec{g'}|^2$ as described in section 3 without the need of specifying the user tolerance ζ. Due to the large number of grid points used in resolving fine scale structures in a typical numerical solution of a hyperbolic PDEs, it is recommended that the each subdomain $\mathbf{\Omega}_k$ be segmented into N_{S_k} subsegment each with m RBF scales before applying the outliers detection algorithm. In [11, 29], it is recommended that the length of local vectors should be in the order of $10 \sim 20$ for a boxplot method to be statistically meaningful. In this paper, we use $m = 20$.

5 RBF shock detection method

By putting all the pieces together, we present the RBF shock detection method.

Algorithm: (RBF shock detection method)

1. Divide the ccomputational domain uniformly into N_S subdomains $\{\mathbf{\Omega}_k\}_{k=1}^{N_S}$ and corresponding overlapping subdomains $\{\mathbf{\Omega}_k^*\}_{k=1}^{N_S}$.

   If, for example, a subdomain $\mathbf{\Omega}_k = [x_{i-N_k}, \cdots, x_i]$, the corresponding overlapping subdomain is $\mathbf{\Omega}_k^* = [x_{i-N_k-n}, \cdots, x_{i-N_k}, \cdots, x_i, \cdots, x_{i+n}]$, which are used to reduce the approximation error at the interface between the subdomains. (In this study, $n = r$).

2. Compute the derivative $\vec{g'}$ of the solution (typically, density ρ) by RBF in $\mathbf{\Omega}_k \subset \mathbf{\Omega}_k^*, k = 1, \cdots, N_S$.

3. Compute $\mathbf{d} = |\vec{g'}|^2$.

4. Segment and detect the non-smooth stencils at each subdomain $\mathbf{\Omega}_k^*$ by the outliers detection algorithm with the mean Q_{mean} being the global mean of $\mathbf{d}$ of the whole physical domain.

Remark 8

1. *To improve the efficiency of the hybrid scheme, for a given function $f(x)$ satisfying the condition $\max\limits_{x \in \mathbf{\Omega}_k^*} f(x) - \min\limits_{x \in \mathbf{\Omega}_k^*} f(x) < 10^{-10}$ in the subdomain $\mathbf{\Omega}_k^*$, we assume $f(x)$ to be a constant and the corresponding subdomain $\mathbf{\Omega}_k^*$ as a smooth stencil directly.*

2. *In this study, the parameters $\epsilon = 0.1, N_k = 100$, are used unless stated otherwise. Note that the shape parameter ϵ in RBF shock detection method with domain decomposition technique cannot be arbitrarily large and should be less than the size of any subdomain $\mathbf{\Omega}_k$, that is, $\epsilon \leq \min\{\epsilon, CN_k\Delta x\}$ where the constant $C \leq 1$. Here we use $C = 1$. The optimal choice of the shape parameter will be studied in the future work.*

In this work, we shall refer to the hybrid Compact-WENO finite difference scheme using the IAMQ-RBF-Fast method without both domain decomposition and outliers detection algorithm as the Hybrid-RBF scheme, with the outliers detection algorithm but without domain decomposition (that is, setting $N_S = 1$ and $\mathbf{\Omega} = \mathbf{\Omega}^*$ in Step 1) as Hybrid-RT, and with both the domain decomposition and outliers detection algorithm as the Hybrid-RTS scheme. In our previous works [5, 6, 10, 11, 21, 34], the multi-resolution (MR) analysis performed well in quantifying the smoothness of a solution computed by the linear scheme and the nonlinear WENO scheme with a uniformly spaced mesh (the Hybrid-MR scheme) and is employed here to provide a context (reference/benchmark) of the performance and behaviors of the Hybrid scheme with RBF shock detection method. We refer to the Hybrid-MR, Hybrid-RBF, Hybrid-RT, Hybrid-RTS schemes collectively as the Hybrid scheme. For clarity, we summarize the Hybrid schemes and their configurations in Table. I.

Table I: Four hybrid schemes and their configurations. The symbol '$\surd$' denotes the techniques employed in the corresponding hybrid scheme.

	Hybrid-RBF	Hybrid-RT	Hybrid-RTS	Hybrid-MR
Edges set definition	$\mathbf{S}_{RBF}$	$\mathbf{S}_{RT}$	$\mathbf{S}_{RT}$	
Domain rescaling	$\surd$	$\surd$	$\surd$	
Levinson-Durbin Algorithm	$\surd$	$\surd$	$\surd$	
Iterative IAMQ-RBF-Fast	$\surd$			
Outlier-detection with Tukey's boxplot method		$\surd$	$\surd$	
Domain decomposition			$\surd$	
Multi-resolution (MR) analysis				$\surd$

6 Numerical Results

To demonstrate the accuracy, robustness, and efficiency of the Hybrid scheme, we show the detailed comparison with those computed by the pure fifth order WENO-Z5 scheme and Hybrid schemes by using classical one- and two-dimensional benchmark problems of the shocked flows. In all the examples, the third order TVD Runge-Kutta method with CFL = 0.45 is used for time integration in solving the system of ODEs resulted from the spatial discretization. For the sake of simplicity,

we will only show the relevant and interesting examples and omit those with simple structures, such as the Lax problem, Sod problem, 123 problem and others.

Two-dimensional Euler equations in a strong conservation form are given as:

$$\mathbf{Q}_t + \mathbf{F}_x + \mathbf{G}_y = 0, \tag{23}$$

with

$$\mathbf{Q} = (\rho, \rho u, \rho v, E)^T,\ \mathbf{F} = (\rho u, \rho u^2 + P, \rho uv, (E+P)u)^T,\ \mathbf{G} = (\rho u, \rho uv, \rho v^2 + P, (E+P)v)^T, \tag{24}$$

where $\mathbf{Q}$ is the conservative variables, $\mathbf{F}$ and $\mathbf{G}$ are the fluxes in the x- and y-directions, and the equation of state is $P = (\gamma - 1)\left(E - \frac{1}{2}\rho(u^2 + v^2)\right)$ with $\gamma = 1.4$. The ρ, u, v, P, and E are the density, velocities in x- and y-directions, pressure, and total energy respectively.

6.1 Two blast-waves interaction problem

First, we will consider the two blast-waves interaction problem, the initial conditions are

$$(\rho, u, P) = \begin{cases} (\ 1,\ 0,\ 1000\ ), & 0.0 \le x < 0.1, \\ (\ 1,\ 0,\ 0.01\ ), & 0.1 \le x \le 0.9, \\ (\ 1,\ 0,\ 100\ ), & 0.9 < x \le 1.0, \end{cases}$$

with $\gamma = 1.4$, $N = 800$ and final time $t = 0.038$. The reflective boundary conditions are imposed on both $x = 0$ and $x = 1$ respectively. In this case, since $\rho(x, 0) = 1$ is a constant, the shock detector methods are employed on both the density ρ and pressure P variables together. The density at the final time and the temporal evolution of WENO `Flag` computed by the Hybrid-RTS scheme are shown in Fig. 3. The hybrid-RTS scheme with the RBF shock detection method captures the shock locations of pressure and density accurately. The solutions are comparable to those in the literature [15, 30].

6.2 Extended Mach 3 Shock-density Wave Interaction Problem

Next, we shall focus on the extended Mach 3 shock-density wave interaction problem which contains the high frequency wave and localized shocklets. This problem allows us to demonstrate the accuracy, robustness, and efficiency of the Hybrid scheme in resolving small scale structures and capturing temporal evolving shocklets.

The initial condition is

$$(\rho, u, P) = \begin{cases} (\ \frac{27}{7},\ \frac{4\sqrt{35}}{9},\ \frac{31}{3}\ ), & -5 \le x < x_0, \\ (\ 1 + \varepsilon\sin(kx),\ 0,\ 1\ ), & x_0 \le x \le 15, \end{cases}$$

where $x \in [-5, 15]$, $\varepsilon = 0.2$, $x_0 = -4$ and $k = 5$, final time $t = 5$.

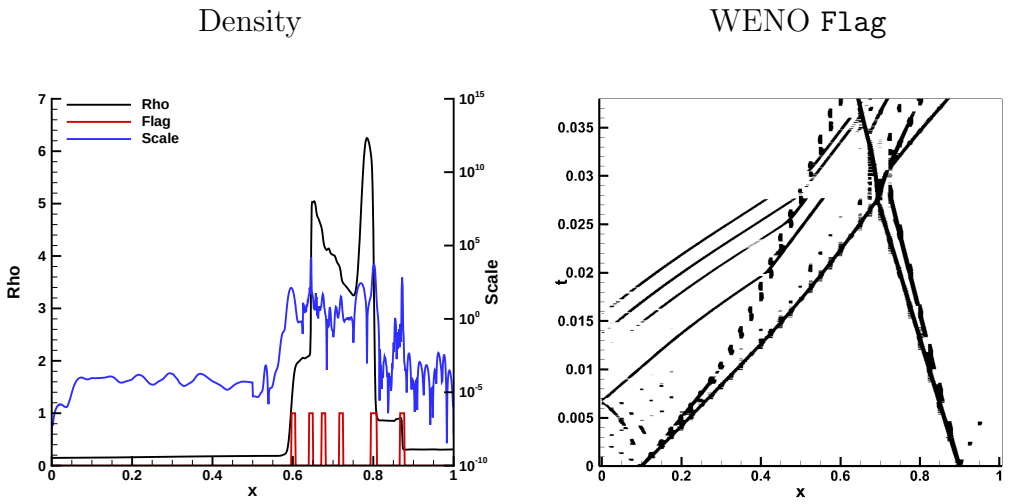

Figure 3: One-dimensional two blast-waves interaction problem with both the density ρ and pressure P being used as the shock detection variables together.

The density ρ at times $t = 2.5$ and $t = 5$, and the temporal evolution of WENO `Flag` computed by the Hybrid-RTS scheme are shown in the left and right figures of Fig. 4 respectively. In this simulation, the algorithm detects the locations of the discontinuities and sharp gradients by using the outliers detection algorithm, resets scales $d_k = \min\{d_k, Q_{\text{mean}}\}$, and then detects for shocks or sharp gradients again. One can easily find that the Hybrid-RTS scheme captures the shocks very accurately. Using the outlier-detection algorithm with the Tukey's boxplot method, the Hybrid-RTS scheme not only detects the shocks as accurately and sharply as the Hybrid-MR scheme but also able to identify the high frequency waves successfully as they are while many shock detection methods, such as the MR analysis, might misidentify them as the high gradients/discontinuities.

Table II shows the CPU times (wall clock in second) and speedup factors in the simulations solved by the WENO-Z5, Hybrid-RBF, Hybrid-RT and Hybrid-RTS schemes with $N = 800$. Due to the ill-condition of the interpolation matrix in the Hybrid-RBF scheme and Hybrid-RT scheme, the shape parameter is $\epsilon = 0.05$. The CPU timing data shows that the Hybrid-RTS scheme is the fastest scheme and about two times faster than the pure WENO-Z5 scheme. However, both the Hybrid-RBF and Hybrid-RT schemes are substantially slower than the WENO-Z5 scheme due to the heavy time consuming in solving the Toeplitz matrix system. Thus, we have omitted the results and CPU timings of the Hybrid-RBF in the rest of the paper as this particular version of hybrid scheme is excessively slow.

6.3 Two-Dimensional Mach 10 Double Mach Reflection Problem

Finally, the two-dimensional Mach 10 double Mach reflection (DMR) problem is considered to illustrate the accuracy and efficiency of the Hybrid-RTS scheme. The computational domain is

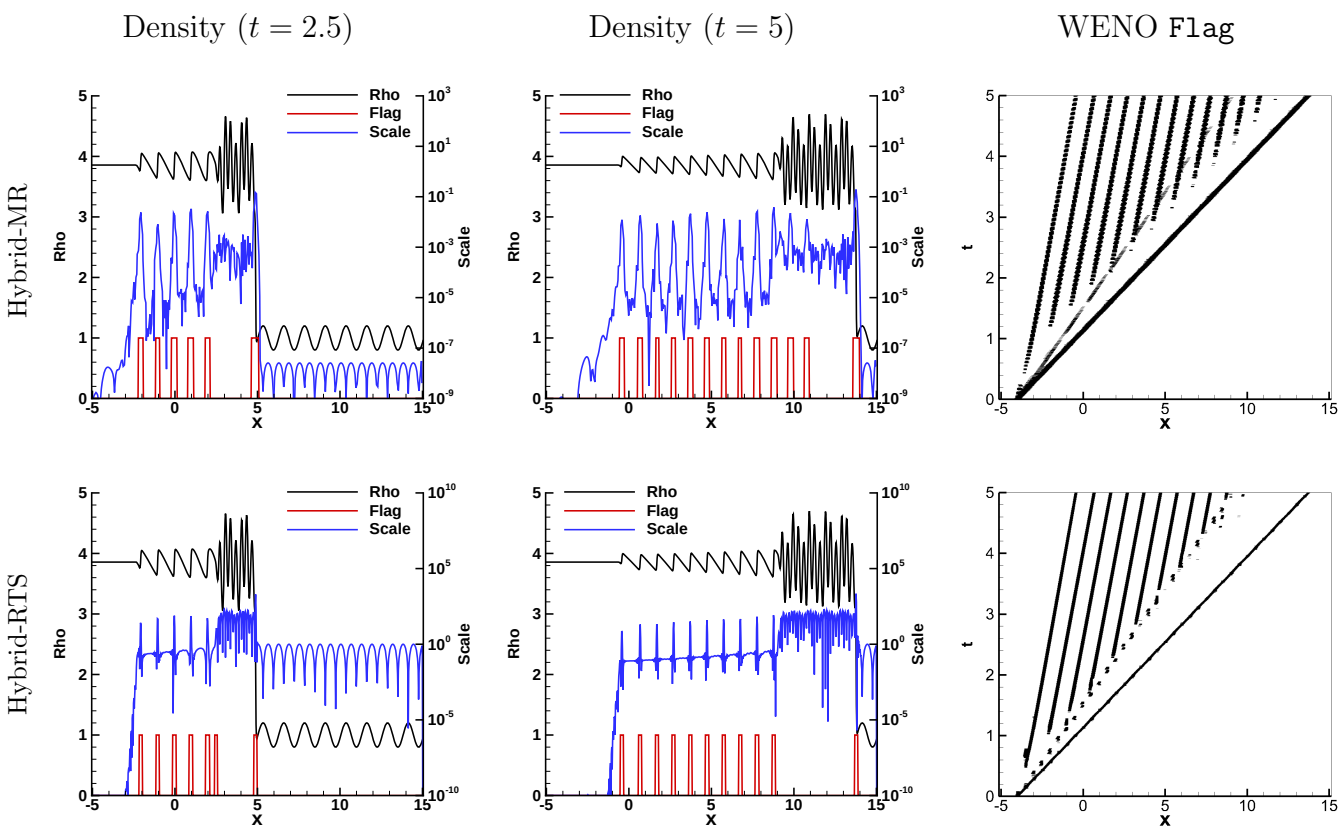

Figure 4: (Color online) (Left) The density at time $t = 2.5$, (Middle) the density at time $t = 5$ and (Right) temporal history of the WENO `Flag` of the extended Mach 3 shock-density wave interaction problem with $N = 800$ computed by (Top) the Hybrid-MR scheme with $\epsilon_{\text{MR}} = 5 \times 10^{-3}$ and (Bottom) the Hybrid-RTS scheme.

Table II: The extended Mach 3 shock-density wave interaction problem. The CPU times (wall clock in second) and speedup factors (SF) of the Hybrid schemes.

N	WENO-Z5	Hybrid-MR		Hybrid-RBF		Hybrid-RT		Hybrid-RTS	
	Time	Time	SF	Time	SF	Time	SF	Time	SF
800	2.2	1.7	1.3	30.5	0.07	3.2	0.7	1.3	1.8
1600	8.7	3.4	2.5	520.0	0.02	17.1	0.5	3.7	2.4
2400	19.2	5.8	3.3	1629.0	0.01	54.7	0.4	7.8	2.5

defined as $[0,4]\times[0,1]$. The initial conditions are

$$Q=(\rho,u,v,P)=\begin{cases}(8,8.25\cos\theta,-8.25\sin\theta,116.5)\,, & x<x_0+y/\sqrt{3},\\ (1.4,0,0,1)\,, & x\geq x_0+y/\sqrt{3},\end{cases}$$

with $x_0=\frac{1}{6}$ and $\theta=\pi/6$. The final time is $t=0.2$. Supersonic inflow and free-stream outflow boundary conditions are specified at $x=0$ and $x=4$, respectively. At the lower boundary $y=0$, reflective boundary conditions are applied in the interval $[x_0,4]$. At the upper boundary $y=1$, the exact solution of the Mach 10 moving oblique shock is imposed. We refer to [30] for the detailed descriptions on the DMR problem.

Fig. 5 shows the colored contour of density and corresponding Flag_x and Flag_y of the DMR problem computed by the Hybrid-MR and Hybrid-RTS schemes, respectively, with the resolution of 800×200. We observe that the Hybrid-RTS scheme captures the shocks and high gradients very well. The small scale structures along the slip line and the vortical rollup at the tip of the jet are much better resolved in the density solution as computed by Hybrid-RTS than the Hybrid-MR. The number of grid points which are flagged as non-smooth stencils is substantially less with the RBF shock detection algorithm indicating the sharp and efficient capturing of the sharp gradients during the evolution of the solution. This fact is also well substantiated by the CPU timings of the problem.

The CPU times along with the speedup in the simulation of DMR problem with the WENO-Z5 scheme, the Hybrid-RT scheme and Hybrid-RTS scheme with resolutions 400×100 and 800×200 are presented in Table III. The data shows that the Hybrid-RTS (Hybrid-RT) scheme is faster than the WENO-Z5 scheme with a speedup factor from ≈2 to ≈3 (≈1.7 to ≈2) as the resolution increases. Compared with the Hybrid-MR scheme, the Hybrid-RTS scheme is at least two times faster than the WENO-Z5 scheme even at the lower resolution.

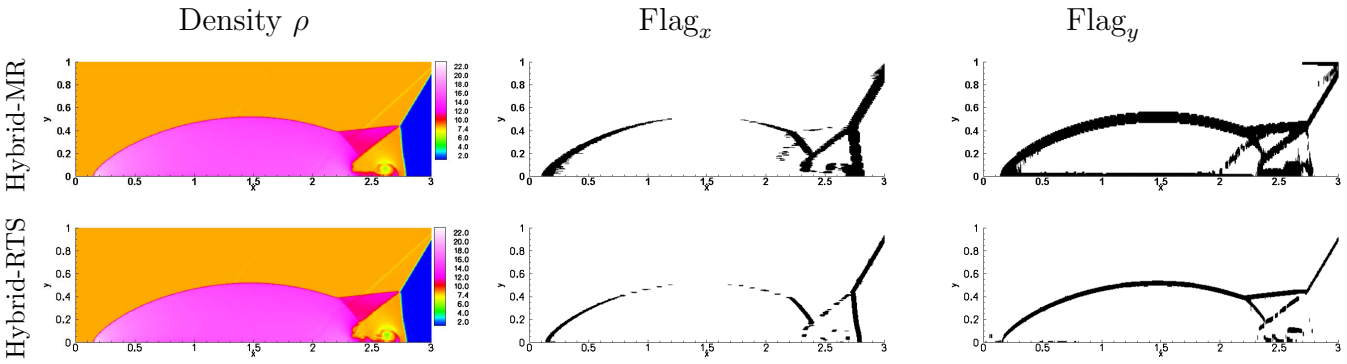

Figure 5: (Color online) DMR problem as computed by Hybrid-MR scheme and Hybrid-RTS scheme with resolution 800×200.

Table III: The CPU timings (wall clock in second) and speedup factors (SF) of the Hybrid scheme.

$N \times M$	WENO-Z5	Hybrid-MR		Hybrid-RT		Hybrid-RTS	
	Time	Time	SF	Time	SF	Time	SF
400×100	144	87	1.7	78	1.9	66	2.2
800×200	1240	539	2.3	756	1.7	430	2.9

6.4 Two-Dimensional Riemann Initial Value Problem

Next, we simulate the classical two-dimensional Riemann problems with initial conditions as follows

$$\mathbf{Q} = (P, \rho, u, v) = \begin{cases} \mathbf{Q}_1 = (P_1, \rho_1, u_1, v_1), & \text{if } x > x_0 \text{ and } y \geq y_0, \\ \mathbf{Q}_2 = (P_2, \rho_2, u_2, v_2), & \text{if } x \leq x_0 \text{ and } y \geq y_0, \\ \mathbf{Q}_3 = (P_3, \rho_3, u_3, v_3), & \text{if } x \leq x_0 \text{ and } y < y_0, \\ \mathbf{Q}_4 = (P_4, \rho_4, u_4, v_4), & \text{if } x > x_0 \text{ and } y < y_0. \end{cases}$$

According to [23], there are 19 genuinely different admissible configurations for polytropic gas, separated by three types of the one-dimensional centered waves, namely, rarefaction-wave($\overrightarrow{R}$), shock-wave($\overleftarrow{S}$), and contact-wave ($J^{\pm}$). The arrows ($\overrightarrow{\cdot}$) and ($\overleftarrow{\cdot}$) indicate forward and backward waves, and the superscript J^+ and J^- refer to negative and positive contacts respectively. The computational configurations are identical to those given in [23] with a resolution of 400×400 and 800×800, with an exception that, in configuration 3, the center is shifted from $(x_0, y_0) = (0.5, 0.5)$ to $(x_0, y_0) = (0.8, 0.8)$ to allow a longer time simulation for a further development of the fine scale structures. We refer readers to [23] for details.

Three representative results of configurations (3, 5, 12) as computed by the Hybrid scheme are demonstrated here. Similar behaviors of the Hybrid scheme are observed in the case of other configurations, and hence, they are omitted.

- **Configuration 3** . $(\overleftarrow{S_{21}}, \overleftarrow{S_{32}}, \overleftarrow{S_{34}}, \overleftarrow{S_{41}})$, $(x_0, y_0) = (0.8, 0.8)$, $t = 0.8$.

$$\mathbf{Q} = \begin{cases} (\ 1.5, & 1.5, & 0, & 0\ ) \\ (\ 0.3, & 0.5323, & 1.206, & 0\ ) \\ (\ 0.029, & 0.138, & 1.206, & 1.206\ ) \\ (\ 0.3, & 0.5323, & 0, & 1.206\ ) \end{cases}$$

- **Configuration 5** . $(\overrightarrow{R_{21}}, \overleftarrow{S_{32}}, \overrightarrow{R_{34}}, \overleftarrow{S_{41}})$, $(x_0, y_0) = (0.5, 0.5)$, $t = 0.23$.

$$\mathbf{Q} = \begin{cases} (\ 1.0, & 1.0, & -0.75, & -0.50\ ) \\ (\ 1.0, & 2.0, & -0.75, & 0.50\ ) \\ (\ 1.0, & 1.0, & 0.75, & 0.50\ ) \\ (\ 1.0, & 3.0, & 0.75, & -0.50\ ) \end{cases}$$

- **Configuration 12**. $(\overrightarrow{S_{21}},\ J_{32}^{+},\ J_{34}^{+},\ \overrightarrow{S_{41}})$, $(x_0, y_0) = (0.5, 0.5)$, $t = 0.25$.

$$\mathbf{Q} = \begin{cases} (\ 0.4,\ 0.5313,\ 0,\ 0\ ) \\ (\ 1,\ 1,\ 0.7276,\ 0\ ) \\ (\ 1,\ 0.8,\ 0,\ 0\ ) \\ (\ 1,\ 1,\ 0,\ 0.7276\ ) \end{cases}$$

In the left figure of Fig. 6, the flooded contours of density of configurations (3, 5, 12) with the resolution of 400×400 as computed by the Hybrid-RTS scheme are shown, respectively. The large scale structures, including the triple point, the incident shock, the reflected shock, a Mach stem and a slip plane, of the flow reach a good agreement with those in the literature [7, 11, 23]. The corresponding Flag_x and Flag_y shown in the middle and right figures of Fig. 6 demonstrate that the Hybrid-RTS scheme captures the discontinuities and sharp gradients accurately. One can easily observe that only a few grid points are contained in the non-smooth domains.

Table IV shows the CPU times along with the speedup factors in the simulation of configurations (3, 5, 12) by the WENO-Z5, Hybrid-MR with $\epsilon_{\text{MR}} = 5 \times 10^{-3}$, Hybrid-RT and Hybrid-RTS schemes with resolutions of 400×400 and 800×800. From the results, the Hybrid-RT scheme is slightly faster than the WENO-Z5 scheme with lower resolution and similar with higher resolution. Similar to the efficiency of Hybrid-MR scheme, the Hybrid-RTS scheme is more than two times faster than the WENO-Z5 scheme under these resolutions.

Table IV: The CPU times (wall clock in second) and speedup factors (SF) of the Hybrid scheme.

Configuration	$N \times M$	WENO-Z5	Hybrid-MR		Hybrid-RT		Hybrid-RTS	
		Time	Time	SF	Time	SF	Time	SF
3	400×400	1922	922	2.1	1073	1.8	833	2.3
	800×800	16040	6038	2.7	15700	1.0	6302	2.6
5	400×400	568	234	2.4	283	2.0	212	2.7
	800×800	4674	1532	3.1	4384	1.1	1535	3.1
12	400×400	628	260	2.4	283	2.2	209	3.0
	800×800	4613	1468	3.1	4300	1.1	1464	3.2

7 Conclusion

In this work, we develop a hybrid compact-WENO finite different scheme with radial basis function (RBF) shock detection method for the discontinuous solutions of hyperbolic conservation laws. To reduce the ill-conditioning of the matrix system as well as to improve the efficiency of the RBF shock detection method, a domain decomposition technique, a novel fast Toeplitz matrix solver, and an

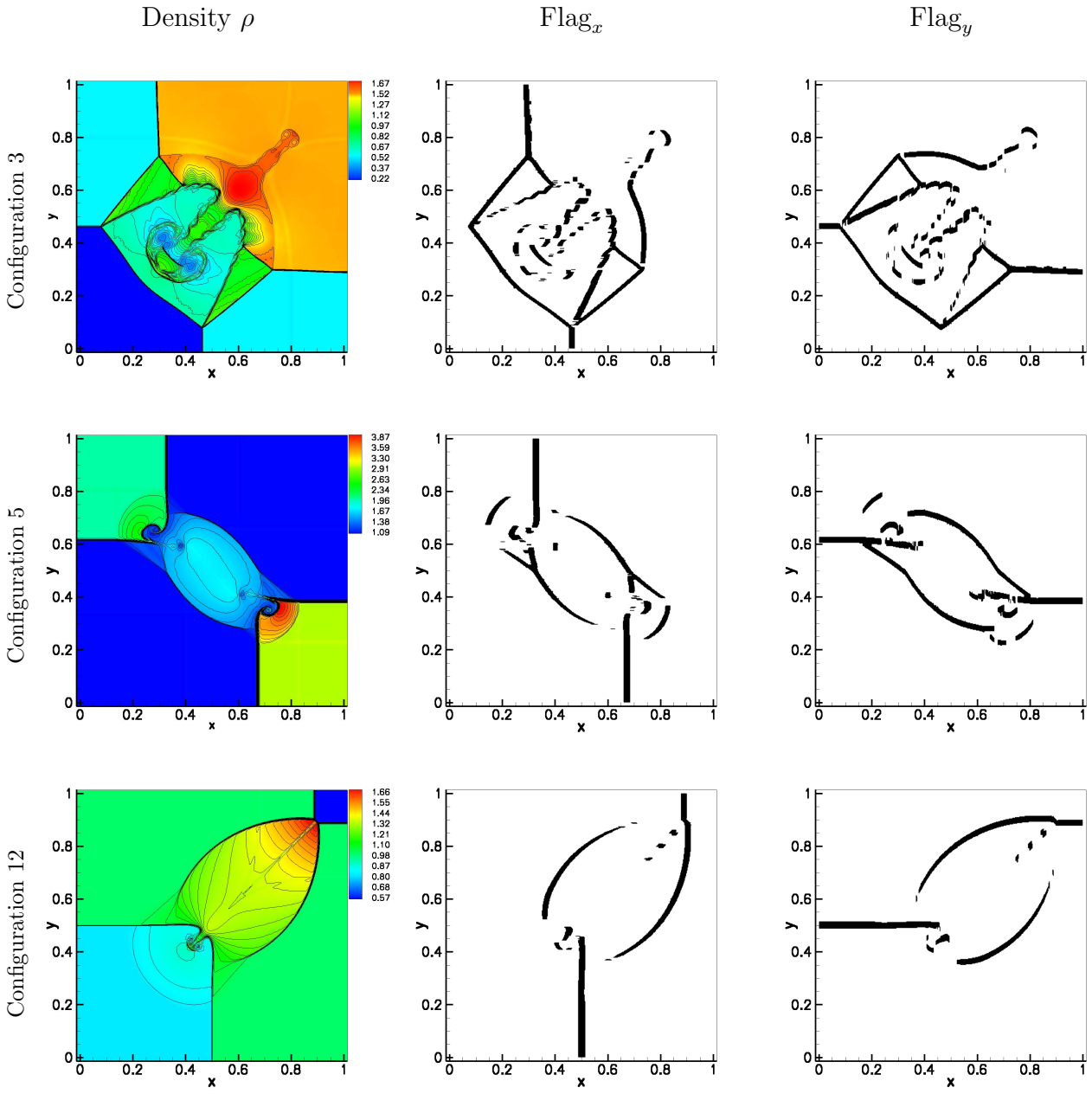

Figure 6: (Color online) (Left) Density ρ, (Middle) Flag$_x$ and (Right) Flag$_y$ identified by the Hybrid-RTS scheme with resolution 400×400 at the final times.

outliers detection algorithm are employed. The extensive numerical examples show that the RBF shock detection method is an accurate, robust, and efficient high order shock detection algorithm which is capable of determining the smoothness of the solution at any given grid point and time. The corresponding hybrid (Hybrid-RTS) scheme not only detects the locations of discontinuous solutions accurately, but also is at least two times faster than the classical fifth order WENO-Z5 scheme in the one- and two-dimensional examples. In summary, speed-wise speaking, the Hybrid-RT scheme (without domain decomposition) is no faster than the WENO-Z5 scheme. The Hybrid-RT scheme is not as competitive as, but the Hybrid-RTS scheme (with domain decomposition) is as efficient as, the Hybrid-MR scheme.

As for the future work, we plan to use the Hybrid-RTS scheme to investigate the reactive Euler equations, the shallow water equations, and the Euler equations under an extreme condition with a strong shock (extreme large density and pressure ratios) and a near vacuum state (extreme low density and pressure).

We note that it is beneficial with respect to accuracy and convergence to add a low order polynomial term in RBF approximation and the optimization of the shape parameter has been studied for smooth problems. The shape parameter plays an critical role in the development of the RBF shock detection method. Therefore, the optimal choice of shape parameter for discontinuous problems will be studied in the future work. In this work, we have assumed that the centers are uniformly distributed, however, the strength of RBF methods is their ability to handle non-uniform grid points. Therefore, the research of RBF shock detection method in a non-uniform or an unstructured mesh for discontinuous Galerkin methods, finite element methods, and finite volume methods, will comprise our future work.

Acknowledgments

The authors would like to acknowledge the funding support of this research by National Science and Technology Major Project (20101010), Shandong Provincial Natural Science Foundation (ZR2017MA016) and Fundamental Research Funds for the Central Universities (201562012). The author (Don) also likes to thank the Ocean University of China for providing the startup funding (201712011) that is used in supporting this work.

References

[1] R. Borges, M. Carmona, B. Costa and W.S. Don, *An improved weighted essentially non-oscillatory scheme for hyperbolic conservation laws*, J. Comput. Phys. **227** (2008) 3191-3211.

[2] M.D. Buhmann, *Radial Basis Functions: Theory and Implementations*, Cambridge University Press, Cambridge, 2003.

[3] M. Castro, B. Costa and W.S. Don, *High order weighted essentially non-oscillatory WENO-Z schemes for hyperbolic conservation laws*, J. Comput. Phys. **230** (2011) 1766–1792.

[4] B. Cockburn and C.-W. Shu, *TVB Runge-Kutta local projection discontinuous Galerkin finite element method for conservation laws II: General framework*, Math. Comput. **52** (1989) 411–435.

[5] B. Costa and W.S. Don, *High order hybrid central-WENO finite difference scheme for conservation laws*, J. Comput. Appl. Math. **204**(2) (2007) 209–218.

[6] B. Costa and W.S. Don, *Multi-domain hybrid spectral-WENO methods for hyperbolic conservation laws*, J. Comput. Phys. **224** (2007) 970–991.

[7] W.S. Don, Z. Gao, P. Li and X. Wen, *Hybrid compact-WENO finite difference scheme with conjugate Fourier shock detection algorithm for hyperbolic conservation laws*, SIAM J. Sci. Comput. **38** (2016) A691–A711.

[8] W.S. Don, B.S. Wang and Z. Gao, *Fast Iterative Adaptive Multi-Quadric Radial Basis Function Method for Edges Detection of Piecewise Functions I : Uniform Mesh*, J. Sci. Comput. DOI 10.1007/s10915-017-0572-y

[9] M. Frigge, D.C. Hoaglin and B. Iglewicz, *Some implementations of the boxplot*, Amer. Statist. **43** (1989) 50–54.

[10] Z. Gao and W.S. Don, *Mapped hybrid central-WENO finite difference scheme for detonation waves simulations*, J. Sci. Comput. **55** (2012) 351–371.

[11] Z. Gao, X. Wen and W.S. Don, *Enhanced robustness of the hybrid Compact-WENO finite difference scheme for hyperbolic conservation laws with multi-resolution analysis and Tukey's boxplot method*, J. Sci. Comput. **73** (2017) 736–752.

[12] A. Harten, *High Resolution Schemes for Hyperbolic Conservation Laws*, J. Comput. Phys. **49** (1983) 357–393.

[13] G. Heinig, K. Rost, *Fast Algorithms for Toeplitz and Hankel Matrices*, Linear Algebra Appl. **435** (2011) 1–59.

[14] D.C. Hoaglin, F. Mosteller and J.W. Tukey, *Understanding robust and exploratory data analysis*, 1st ed., Wiley Series in Probability and Mathematical Statistics, Wiley, 1983.

[15] X. Y. Hu, N. A. Adams and C.-W. Shu, *Positivity-preserving method for high-order conservative schemes solving compressible Euler equations*, J. Comput. Phys. **242** (2013) 169–180.

[16] G.S. Jiang and C.-W. Shu, *Efficient implementation of weighted ENO Schemes*, J. Comput. Phys. **126** (1996) 202–228.

[17] J.-H. Jung and V. Durante, *An iterative multiquadric radial basis function method for the detection of local jump discontinuities*, Appl. Numer. Math. **59** (2009) 1449–1446.

[18] J.-H. Jung, S. Gottlied and S.O. Kim *Iterative adaptive RBF methods for detection of edges in two-dimensional functions*, Appl. Numer. Math. **61** (2011) 77–91.

[19] E.J. Kansa, *Exact explicit time integration of hyperbolic partial differential equations with mesh free radial basis functions*, Eng. Anal. Bound. Elem. **31** (2007) 577–585.

[20] L. Krivodonova, J. Xin, J.-F. Remacle, N. Chevaugeon and J. Flaherty, *Shock detection and limiting with discontinuous Galerkin methods for hyperbolic conservation laws*, Appl. Numer. Math. **48** (2004) 323–338.

[21] P. Li, W.S. Don, C. Wang and Z. Gao, *High Order Positivity- and Bound-Preserving Hybrid Compact-WENO Finite Difference Scheme for the Compressible Euler Equations*, J. Sci. Comput. (2017) doi:10.1007/s10915-017-0452-5.

[22] P. Li, Z. Gao, W.S. Don and S.S. Xie, *Hybrid Fourier-Continuation Method and Weighted Essentially Non-oscillatory Finite Difference Scheme for Conservation Laws in a Single-Domain Framework*, J. Sci. Comput. **64** (2015) 670–695.

[23] C.W. Schulz-Rinne, *Classification of the Riemann problem for two-dimensional gas dynamics*, SIAM J. Math. Anal. **24** (1993) 76–88.

[24] C.-W. Shu, *High order weighted essentially nonoscillatory schemes for convection dominated problems*, SIAM Rev. **51**(1) (2009) 82–126.

[25] W. Trench, *An Algorithm for the Inversion of Finite Toeplitz Matrices*, SIAM J. Appl. Math. **12** (1964) 515–522.

[26] J.W. Tukey, *Exploratory data analysis*, 1st ed., Behavioral Science: Quantitative Methods, Addison-Wesley, 1977.

[27] O. Vasilyev, T. Lund and P. Moin, *A general class of commutative filters for LES in complex geometries*, J. Comput. Phys. **146**(1) (1998) 82–104.

[28] P.F. Velleman and D.C. Hoaglin, *Applications, basics, and computing of exploratory data analysis*, Duxbury Press, Boston, 1981.

[29] M.J. Vuik and J.K. Ryan, *Automated parameters for troubled-cell indicators using outlier detection*, SIAM J. Sci. Comput. **38** (2016) A84–A104.

[30] P. Woodward and P. Collela, *The numerical simulation of two dimensional fluid flow with strong shocks*, J. Comput. Phys. **54** (1984) 115–173.

[31] P.V. Yee and S. Haykin, *Regularized Radial Basis Function Networks: Theory and Applications*, John Wiley & Sons, Inc., New York, 2001.

[32] J. Yoon, *Spectral approximation orders of radial basis function interpolation on the Sobolev space*, SIAM J. Math. Anal. **33** (2001) 946–958.

[33] X. Zhou, Y.C. Hon and J. Li, *Overlapping domain decomposition method by radial basis functions*, Appl. Numer. Math. **44** (2003) 241–255.

[34] Q.Q. Zhu, Z. Gao, W.S. Don and X.Q. Lv, *Well-balanced Hybrid Compact-WENO Schemes for Shallow Water Equations*, Appl. Numer. Math. **112** (2017) 65–78.